Emitter-Active Shell in NaYF4:Yb,Er/NaYF4:Er Upconversion Nanoparticles for Enhanced Energy Transfer in Photodynamic Therapy

Ren, J.; Ding, Y.; Zhu, H.; Li, Zhipeng; Dai, R.; Zhao, H.; Hong, X.; Zhang, H.

DOI
10.1021/acsanm.1c03377

Publication date
2022

Document Version
Final published version

Published in
ACS Applied Nano Materials

ACS APPLIED NANO MATERIALS

www.acsanm.org Article

Emitter-Active Shell in $NaYF_4$:Yb,Er/$NaYF_4$:Er Upconversion Nanoparticles for Enhanced Energy Transfer in Photodynamic Therapy

Jie Ren, Yadan Ding,* Hancheng Zhu, Zhipeng Li, Rui Dai, Huiying Zhao, Xia Hong,* and Hong Zhang*

Cite This: *ACS Appl. Nano Mater.* 2022, 5, 559−568 Read Online

ACCESS | Metrics & More | Article Recommendations | Supporting Information

ABSTRACT: To realize the potential of near-infrared (NIR) upconversion nanosensitizers for photodynamic therapy of cancer, upconversion luminescence and energy transfer (ET) efficiency from emitter donors to photosensitizer acceptors need to be improved. In the current work, upconversion nanoparticles (UCNPs) with a core/emitter-active shell structure were constructed to enhance not only the upconversion emission but also the ET from the nanoparticles to surface-anchored photosensitizers. The emitter was doped into the shell to bridge the migration of upconverted energy to the surface. $NaYF_4$:Yb,Er/$NaYF_4$:Er UCNPs and rose bengal (RB) photosensitizer were employed as an example. The upconversion emission was lifted by up to ∼81 times of the core counterpart. The bridge effect of the emitter-doped shell was obvious for the constructed nanophotosensitizer. The emission of the RB photosensitizer was up to ∼36 times that of the core counterpart. The $NaYF_4$:Yb,Er/$NaYF_4$:Er UCNPs also endow the RB photosensitizers with the most efficient reactive oxygen species production capability under NIR irradiation. In vitro photodynamic tests on glioma cells were conducted to validate the efficacy of the $NaYF_4$:Yb,Er/$NaYF_4$:Er/RB agent. Therefore, this work can facilitate the development of ET-based upconversion nanosystems.

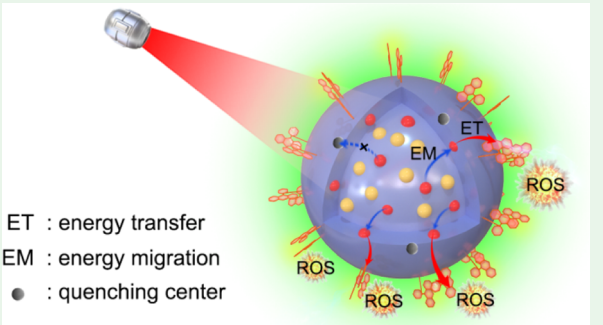

KEYWORDS: *upconversion nanoparticles, photosensitizer, energy transfer, core/shell, photodynamic therapy*

1. INTRODUCTION

Photodynamic therapy (PDT) is a promising therapeutic modality for cancer which threatens human health seriously. PDT can damage localized cancer cells using toxic reactive oxygen species (ROS) generated by light-triggered photosensitizers in the presence of oxygen.[1−4] Compared with traditional therapeutic methods, including surgery, radiotherapy, and chemotherapy, PDT exhibited advantages of low systematic toxicity, high selectivity, and minimal invasiveness.[5,6] However, the application of PDT has been significantly hindered because photosensitizers are usually triggered by ultraviolet (UV) or visible light, which are susceptible to absorption and scattering and thus have shallow penetration in biological tissues.[1,7] Therefore, there is an emerging need to develop near-infrared (NIR) light-excitable photodynamic therapeutic agents.

Rare earth-doped upconversion nanoparticles (UCNPs) are capable of converting NIR excitation light to UV and visible emission light and thus provide a great opportunity.[8−10] UCNPs are featured in strong photobleaching resistance, deep tissue penetration, and negligible background fluorescence.[11,12] By transferring upconverted excitation energy to the adjacent photosensitizer, UCNPs can serve as NIR light transducers of photodynamic therapeutic agents.[13−15] To realize the potential of UCNPs for the therapy of deep lesions, the upconversion luminescence and energy transfer (ET) efficiency from emitter donors to surface-anchored photosensitizer acceptors need to be improved. ET efficiency decreases sharply as the donor−acceptor distance increases. Therefore, efforts have been focused mainly on bare-core-structured UCNPs (e.g., $NaYF_4$:Yb,Er and $NaYF_4$:Yb,Gd,Tm) to minimize the distance between energy donors (emitter ions in the UCNPs, e.g., Er^{3+} and Tm^{3+}) and photosensitizer acceptors.[16−18]

Shell coating can effectively enhance the luminescence intensity of UCNPs.[19−22] Inspired by this, we demonstrated previously theoretically and experimentally that an inert shell with an appropriate thickness can improve ET from the

Received: October 12, 2021
Accepted: December 7, 2021
Published: December 16, 2021

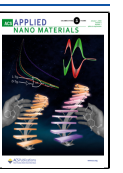

https://doi.org/10.1021/acsanm.1c03377
ACS Appl. Nano Mater. 2022, 5, 559−568

UCNPs to the surface-bound acceptor.[23,24] In the past few years, core/shell structured UCNPs, such as $LiYF_4$:Er/$LiGdF_4$, $NaYF_4$:Yb,Er,Gd/$NaYF_4$:Gd, $NaGdF_4$:Yb,Er,Mn/$NaGdF_4$:Yb and $NaYF_4$:Yb,Tm/$NaYF_4$:Yb/$NaNdF_4$:Yb/$NaYF_4$, have attracted growing interest for the development of ET systems.[25−33] The introduction of one or more inert or sensitizer-active shells significantly improves the upconversion luminescence. However, the shell can increase the distance between the inner emitters and the photosensitizing molecules at the surface, thus reducing the ET efficiency. The donor−acceptor distance can be shortened by constructing various unique core/shell structures with the emitter also in the shell, such as $NaYF_4$:Yb/$NaYF_4$:Yb,Er,[34] $NaLiF_4$:Yb/$NaLiF_4$:Yb,Tm,[35] $NaGdF_4$/$NaGdF_4$:Yb,Er,[36] $NaYF_4$:Nd,Yb/$NaYF_4$:Yb/$NaYF_4$:Yb,Tm,[37] $NaYbF_4$/$NaYF_4$:Gd,Er/$NaYF_4$:Gd,[38] and $NaYF_4$:Nd,Yb/$NaYF_4$:Yb/$NaYF_4$:Yb,Er/$NaYF_4$.[39] Despite these advances, the outermost shell can directly expose the emitter to the external environment or separate the emitter from the surface acceptor, thus reducing the upconversion luminescence and/or the ET efficiency. Therefore, a sweet spot between upconversion luminescence and ET efficiency needs to be identified to promote the practical applications of NIR upconversion nanosensitizers in PDT.

In this work, new NIR light excitable PDT nanoagents were constructed using $NaYF_4$:Yb,Er/$NaYF_4$:Er as the core/emitter-active-shell structured UCNPs and rose bengal (RB) as the photosensitizer. $NaYF_4$ shell was applied to enhance the upconversion luminescence by surface passivation, and Er^{3+} was introduced into the shell to bridge ET from the Er^{3+} emitter in the core to the surface-anchored RB acceptor. The concentration of Er^{3+} in the shell and the shell thickness were optimized to achieve the best RB efficacy. The developed $NaYF_4$:Yb,Er/$NaYF_4$:Er UCNPs exhibited the strongest RB emission and produced the highest amount of ROS under 980 nm excitation, compared with control groups of different structures and doping patterns. In vitro photodynamic killing of glioma cells was carried out as a proof of principle.

2. EXPERIMENTAL SECTION

2.1. Reagents and Instrumentation. Details of the reagents and instruments used for material characterization are provided in the Supporting Information.

2.2. Synthesis of $NaYF_4$: 20% Yb, 2% Er/$NaYF_4$: *x* % Er (*x* = 0−5.0) UCNP. Oleate-capped $NaYF_4$: 20% Yb, 2% Er/$NaYF_4$: *x* % Er (*x* = 0−5.0) UCNPs were prepared following reported protocols of $NaYF_4$:Yb,Er/$NaYF_4$.[40] The concentration of Er^{3+} doped in the shell was adjusted by preparing sacrificial nanocrystals with the stoichiometric mixture of $Y(CF_3COO)_3$ and $Er(CF_3COO)_3$ instead of $Y(CF_3COO)_3$. Core $NaYF_4$:Yb,Er UCNPs were synthesized by heating YCl_3/$YbCl_3$/$ErCl_3$ (0.78 mmol/0.20 mmol/0.02 mmol) in oleic acid (OA, 6 mL) and 1-octadecene (ODE, 15 mL) to 160 °C under a N_2 flow, and the mixture was held under those conditions for 30 min. After cooling to 50 °C, 5 mL of methanol containing NaOH/NH_4F (2.5 mmol/4.0 mmol) was added to the mixture, heated to 85 °C, and held at that temperature for 100 min. After the mixture was allowed to react at 310 °C for 90 min, a portion of the resulting core sample was collected with a syringe. Sacrificial nanocrystals were injected into the reaction mixture, and a core/shell sample was obtained after ripening. Core/shell samples with increasing thicknesses (from CS1 to CS8) were obtained by repeating the process of sacrificial nanocrystal injecting, ripening, and sample collecting. The samples were washed with ethanol/acetone three times and dispersed in cyclohexane.

2.3. Preparation of UCNP/RB Therapeutic Agents. UCNPs (1 mL, ∼10 mg/mL) were mixed with HCl (0.05 M), and the mixture was stirred for 24 h to remove the oleate ligand. After they were washed with isopropanol and dispersed in water, 50 μL of poly(allylamine) (PAAM) was added, and the mixture was stirred for 20 h to further modify UCNPs with amino groups. To incorporate the RB photosensitizer to the UCNPs covalently, 10 μg/mL of carboxyl-modified RB (RB-HA)[41] was first reacted with *N*-(3-dimethylaminopropyl)-*N*′-ethylcarbodiimide hydrochloride (EDC, 100 μg/mL) and *N*-hydroxysulfosuccinimide sodium salt (NHS, 100 μg/mL) for 2 h. Then, 0.5 mL of UCNP/PAAM (∼0.14 nmol/mL, estimated according to the size and density of hexagonal $NaYF_4$) was added and reacted for a further 24 h. The resulting UCNP/RB was washed several times using dimethylsulfoxide (DMSO) and stored in DMSO.

2.4. Detection of ROS. A dimethyl formamide solution was prepared by mixing 1,3-diphenylisobenzofuran (DPBF, 20 μL, 10 mM) with 1 mL of RB, ∼22 nm $NaYF_4$:Yb,Er/PAAM, ∼42 nm $NaYF_4$:Yb,Er/PAAM, ∼42 nm $NaYF_4$:Yb,Er/$NaYF_4$/PAAM, ∼42 nm $NaYF_4$:Yb,Er/$NaYF_4$: 0.5% Er/PAAM, and the conjugates of the above UCNPs with RB, respectively. The concentrations of UCNP/PAAM and UCNP/RB were all ∼0.14 nmol/mL. The mixtures were then irradiated with a 980 nm laser (0.7 W/cm^2) in the dark. The absorbance at 417 nm was recorded every 5 min.

2.5. Cytotoxicity of UCNP/RB Therapeutic Agents. Glioma cells (U87MG cell line) were used to study the cytotoxicity of the conjugates of RB and the four types of UCNPs, which were ∼22 nm $NaYF_4$:Yb,Er, ∼42 nm $NaYF_4$:Yb,Er, ∼42 nm $NaYF_4$:Yb,Er/$NaYF_4$, and ∼42 nm $NaYF_4$:Yb,Er/$NaYF_4$: 0.5% Er. The cells were cultured at 37 °C in Dulbecco's modified Eagle's medium (DMEM), which contained streptomycin (100 μg/mL), penicillin (100 U/mL), and fetal blood serum (10%). The culture medium was removed after the cells were seeded into 96-well plates (10^4 cells/well) and incubated for 24 h. Subsequently, 100 μL of the UCNP/RB therapeutic agents dispersed in DMEM at various concentrations were added into the wells and incubated for 24 h. After adding the cell counting kit-8 (CCK-8, 10 μL) reagent and culturing for another 2 h, the absorbance at 450 nm was recorded with a microplate spectrophotometer (WELLSCAN MK3, Labsystems Dragon, America) to calculate cell viability.

Flow cytometric analysis was also performed to evaluate the cytotoxicity of the UCNP/RB therapeutic agents toward U87MG cells. DMEM was removed after U87MG cells were seeded into six-well plates and incubated for 24 h. Then, 500 μg/mL of UCNP/RB therapeutic agents (including ∼22 nm $NaYF_4$:Yb,Er/RB, ∼42 nm $NaYF_4$:Yb,Er/RB, ∼42 nm $NaYF_4$:Yb,Er/$NaYF_4$/RB, and 42 nm $NaYF_4$:Yb,Er/$NaYF_4$:Er/RB) dispersed in DMEM were added into the wells. After incubation for 24 h, U87MG cells were harvested with trypsin (0.05%) and washed twice using phosphate-buffered saline (PBS). Afterward, 1×10^5 cells in binding PBS (100 μL) containing calf serum (10%) were added to a centrifuge tube (1.5 mL) and incubated with Annexin-V-fluorescein isothiocyanate (5 μL) and propidium iodide (PI, 5 μL) for 20 min in the dark. After it was washed twice with PBS, the cell suspension was used for flow cytometric analysis (BD FACSCalibur, America).

2.6. Intracellular ROS Production by UCNP/RB Therapeutic Agents. U87MG cells were seeded into 96-well plates (10^4 cells/well), incubated for 24 h, and then divided into 15 groups. These groups are (1) the control group, (2) NIR light irradiation, (3) RB + NIR light irradiation, (4) ∼22 nm $NaYF_4$:Yb,Er/PAAM + NIR light irradiation, (5) ∼42 nm $NaYF_4$:Yb,Er/PAAM + NIR light irradiation, (6) ∼42 nm $NaYF_4$:Yb,Er/$NaYF_4$/PAAM + NIR light irradiation, (7) ∼42 nm $NaYF_4$:Yb,Er/$NaYF_4$: 0.5% Er/PAAM + NIR light irradiation, (8) ∼22 nm $NaYF_4$:Yb,Er/RB, (9) ∼42 nm $NaYF_4$:Yb,Er/RB, (10) ∼42 nm $NaYF_4$:Yb,Er/$NaYF_4$/RB, (11) ∼42 nm $NaYF_4$:Yb,Er/$NaYF_4$:Er/RB, (12) ∼22 nm $NaYF_4$:Yb,Er/RB + NIR light irradiation, (13) ∼42 nm $NaYF_4$:Yb,Er/RB + NIR light irradiation, (14) ∼42 nm $NaYF_4$:Yb,Er/$NaYF_4$/RB + NIR light irradiation, and (15) ∼42 nm $NaYF_4$:Yb,Er/$NaYF_4$:Er/RB + NIR light irradiation. The original culture media in group 3, groups 4−7, and groups 8−15 were replaced with 100 μL of fresh culture media containing RB, UCNP/PAAM, and UCNP/RB therapeutic agents

https://doi.org/10.1021/acsanm.1c03377
ACS Appl. Nano Mater. 2022, 5, 559−568

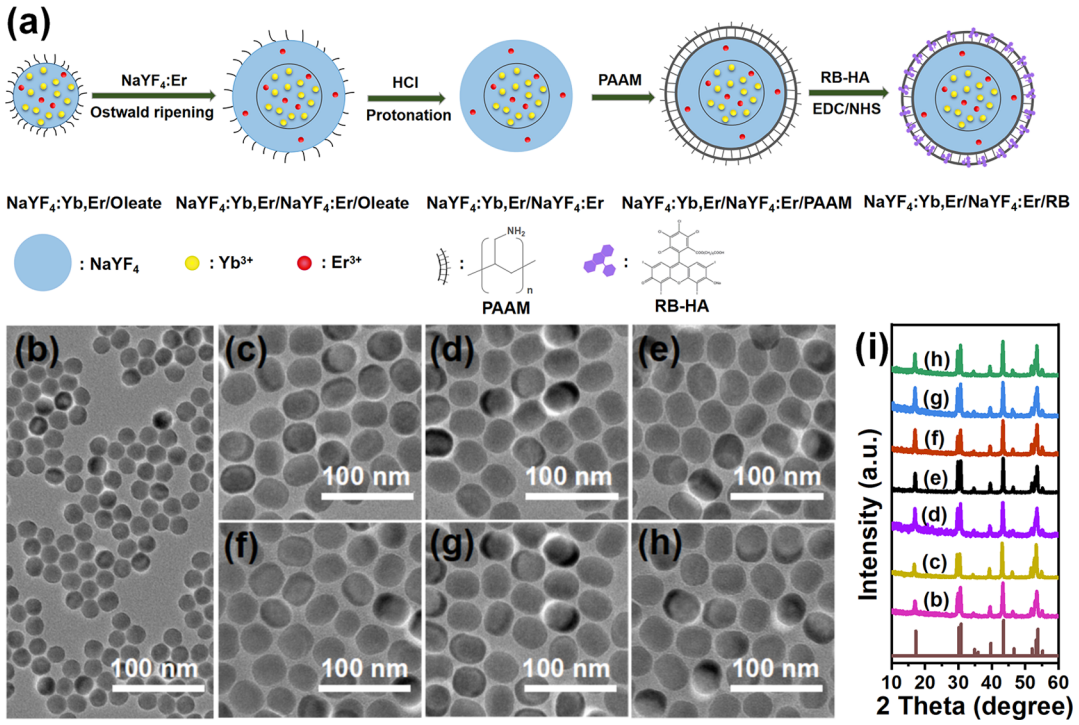

Figure 1. (a) Schematic of synthesis of $NaYF_4$:Yb,Er/$NaYF_4$:Er/RB therapeutic agents. TEM images of (b) $NaYF_4$:Yb,Er/oleate and $NaYF_4$:Yb,Er/$NaYF_4$:Er/oleate with (c) 0.0, (d) 0.2, (e) 0.5, (f) 1.0, (g) 2.0, and (h) 5.0% Er^{3+} in the shell. (i) XRD patterns of UCNPs corresponding to those in (b–h). Standard data of hexagonal $NaYF_4$ (JCPDS card no. 16-0334) is presented for reference.

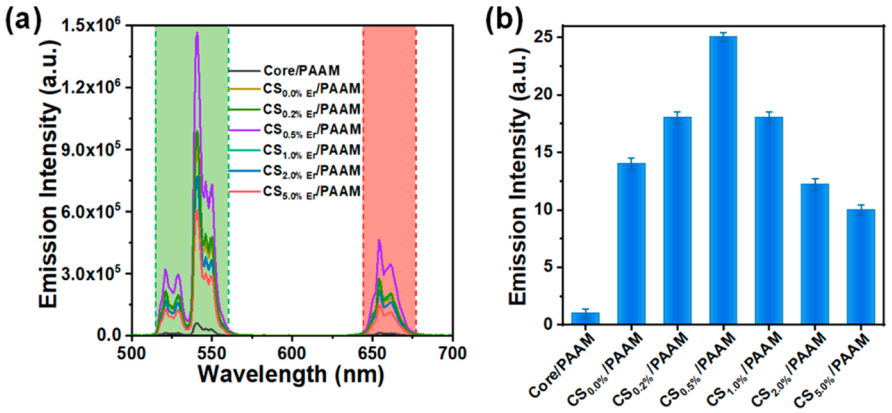

Figure 2. (a) Emission spectra and (b) integrated emission intensities of $NaYF_4$:Yb,Er/PAAM and $NaYF_4$:Yb,Er/$NaYF_4$:Er/PAAM with various concentrations of Er^{3+} in the shell under 980 nm excitation.

(500 μg/mL), respectively. After the cells were cultured for another 4 h in the new media, groups 2–7 and 12–15 were exposed to a 980 nm laser (0.7 W/cm^2) for 10 min. 2′,7′-Dichlorodihydrofluorescein diacetate (DCFH-DA, 10 μL) reagent was then added to each well and incubated for 20 min. After being washed with PBS three times, the cells were imaged using a fluorescence microscope.

2.7. Photodynamic Killing of Cancer Cells with UCNP/RB Therapeutic Agents. The viability of U87MG cells in the aforementioned 15 groups described in Section 2.6 was first used to indicate the photodynamic therapeutic efficacy of UCNP/RB therapeutic agents. After NIR treatment (0.7 W/cm^2) for 10 min, a CCK-8 reagent (10 μL), instead of DCFH-DA, was added to the wells and incubated for 2 h. The absorbance at 450 nm was recorded to calculate cell viability. U87MG cells treated with conditions described in Section 2.6 were then observed with a fluorescent microscope after they were stained with calcein-AM/PI solutions for 20 min and washed with PBS three times.

2.8. Statistical Analysis. Student's *t*-test was used to evaluate statistical significance. $^*p < 0.05$, $^{**}p < 0.01$, and $^{***}p < 0.001$ were considered statistically significant. Data are shown as mean ± standard deviation ($n = 3$).

3. RESULTS AND DISCUSSION

3.1. Construction of UCNP/RB Therapeutic Agents. The synthesis procedures of the core/emitter-active shell UCNP/RB therapeutic agents are presented in Figure 1a. Typical 20% Yb^{3+}, 2% Er^{3+} codoped $NaYF_4$ UCNPs were first synthesized as the core in solvents with high boiling points (OA/ODE).[42,43] Er^{3+}-doped $NaYF_4$ was then coated by Ostwald ripening according to a reported procedure.[40] To anchor the RB photosensitizer on UCNPs, as-prepared UCNPs were treated with HCl to remove the oleate ligand and further modified with amino-abundant PAAM. Finally, the amino-modified UCNPs were incorporated with carboxyl-

https://doi.org/10.1021/acsanm.1c03377
ACS Appl. Nano Mater. 2022, 5, 559–568

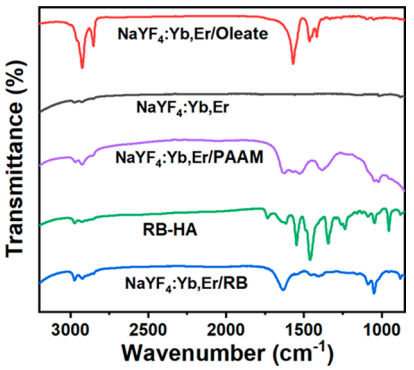

Figure 3. FTIR spectra of oleate-capped UCNPs, bare UCNPs, amino-modified UCNPs, carboxyl group-modified RB, and the UCNP/RB therapeutic agents.

modified RB through EDC/NHS crosslinking. The UCNPs can transfer upconverted excitation energy to surface-bound RB molecules, which then produce cytotoxic ROS.

The transmission electron microscope (TEM) images of $NaYF_4$:Yb,Er core structured UCNPs and $NaYF_4$:Yb,Er/$NaYF_4$:Er core/shell structured UCNPs with various concentrations of Er^{3+} in the shell are shown in Figure 1b–h. All the samples were quasi-spherical in shape. The core UCNPs were approximately 22 nm in diameter, and the core/shell UCNPs with various Er^{3+} doping concentrations were all approximately 32 nm in diameter. Thus, the shell thickness was ~5 nm. Dynamic light scattering (DLS) results indicated a narrow size distribution of as-prepared UCNPs (Figure S1). The actual doping concentrations of Yb^{3+} and Er^{3+} in $NaYF_4$:Yb,Er core were determined to be 19.0 and 2.1%, respectively, using inductively coupled plasma analysis, and an increasing amount of Er^{3+} was also confirmed from the $NaYF_4$:Yb,Er/$NaYF_4$:Er samples with an increasing concentration of Er^{3+} in the shell (Table S1). X-ray diffraction (XRD) patterns (Figure 1i) indicated that these UCNPs were in the hexagonal phase, a more effective crystal phase than its cubic counterpart for enhanced upconversion efficiency.[44,45]

Upconversion luminescence of the UCNPs was investigated under 980 nm excitation. As shown in Figure 2, two green emission peaks centered at 520 and 540 nm and one red emission peak centered at 655 nm appeared. They were ascribed to $^2H_{11/2}$, $^4S_{3/2}$, and $^4F_{9/2}$ transitions to $^4I_{15/2}$ in Er^{3+}, respectively. The upconversion luminescence of $NaYF_4$:Yb,Er was enhanced by one order of magnitude after it was coated by an inert shell of $NaYF_4$. It resulted from efficient surface passivation of Er^{3+} emitters from surface defects, ligand, solvent, and so on.[46,47] As the concentration of the Er^{3+} emitters doped in the $NaYF_4$ shell gradually increased to 0.5%, the upconversion luminescence intensity further increased. It indicated that Er^{3+} in the shell can also act as a normal emitter to produce upconversion luminescence. However, when Er^{3+} concentration in the shell continued to increase, the luminescence intensity declined. It implied that the upconverted excitation energy can dissipate to the surface via Er^{3+} in the shell. That is, the surface passivation effect of the shell was suppressed. Thus, it is essential to control the concentration of Er^{3+} doped in the shell to enhance not only the upconversion emission but also the ET to surface-anchored entities.

The coupling process of core/emitter-active-shell UCNPs with the RB photosensitizers was verified using Fourier-transform infrared (FTIR) spectroscopy (Figure 3). There were four main absorption peaks corresponding to oleate-capped UCNPs. They were centered at around 2930, 2850, 1570, and 1470 cm^{-1}, which originated from stretching vibrations of $-CH_2$ and $-CH_3$ and asymmetric and symmetric stretching vibrations of carboxylate anions, respectively. These absorption peaks disappeared after the oleate ligand was removed. Successful PAAM modification was verified by the appearance of two absorption peaks originating from the bending vibration of N–H (1580 cm^{-1}) and stretching vibration of C–N (1113 cm^{-1}). The resulting size increase (~7 nm) relative to the bare UCNPs was also observed in the DLS measurements (Figure S2). Two absorption peaks resulting from the stretching vibration of C═O (1725 cm^{-1}) and deformation vibration of –OH (950 cm^{-1}) in the carboxyl groups were observed from RB-HA. After it was conjugated with the UCNPs, the two absorption peaks disappeared, and an additional absorption peak was observed at 1634 cm^{-1}. The new peak originated from the stretching vibration of C═O in the amide group, indicating that covalent interactions existed between UCNPs and the RB photosensitizer. The centrifugal supernatant was analyzed, and the number of RB photosensitizers coupled onto the surface of each $NaYF_4$:Yb,Er/$NaYF_4$:Er core/shell structured UCNP with various concentrations of Er^{3+} in the shell was estimated to be approximately 290 ± 18. Thus, similar amounts of RB can be incorporated into the system under the same conditions.

The upconversion luminescence spectra of the UCNP/RB therapeutic agents with various doping concentrations of Er^{3+}

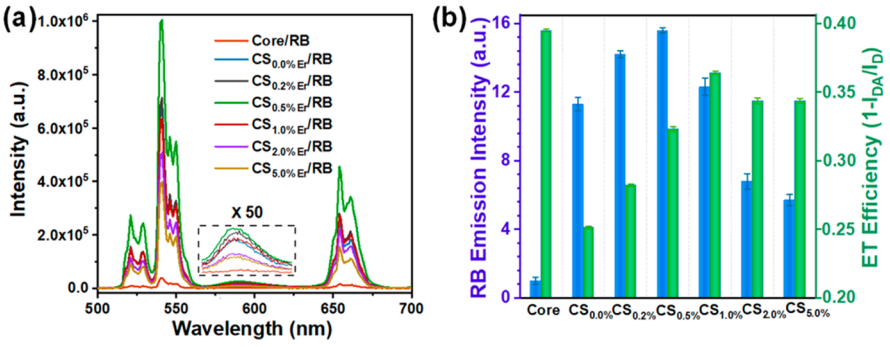

Figure 4. (a) Emission spectra of UCNP/RB therapeutic agents under 980 nm excitation. (b) RB emission intensities integrated in the range of 565–630 nm from (a) and ET efficiency of UCNP/RB therapeutic agents. Intensity of red emission was used as an internal reference for calculating ET efficiency.

https://doi.org/10.1021/acsanm.1c03377
ACS Appl. Nano Mater. 2022, 5, 559–568

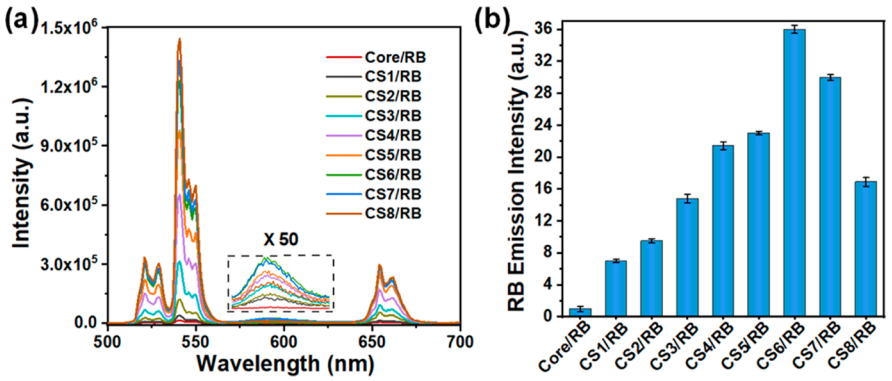

Figure 5. (a) Emission spectra of $NaYF_4$:Yb,Er/$NaYF_4$:Er/RB therapeutic agents with various shell thicknesses under 980 nm excitation. (b) RB emission intensities integrated in the range of 565−630 nm from (a).

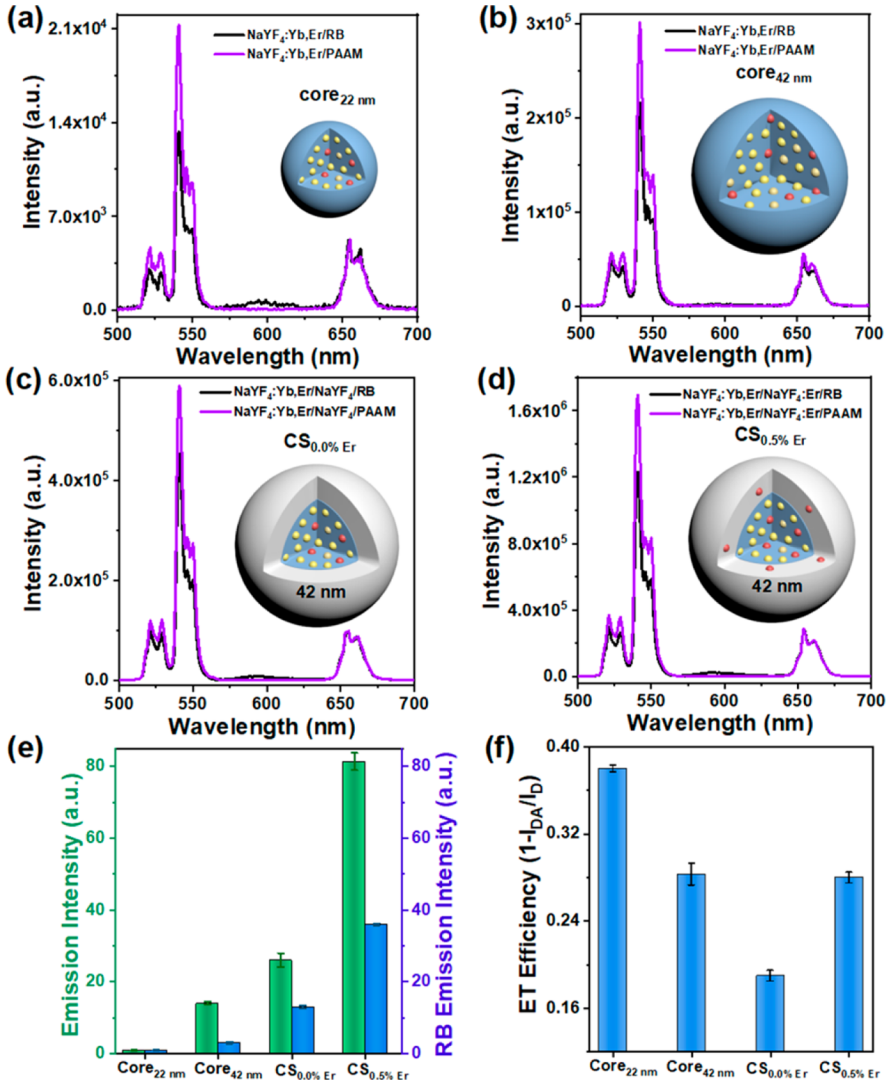

Figure 6. Emission spectra of (a) ∼22 nm $NaYF_4$:Yb,Er/PAAM, (b) ∼42 nm $NaYF_4$:Yb,Er/PAAM, (c) ∼42 nm $NaYF_4$:Yb,Er/$NaYF_4$/PAAM, and (d) ∼42 nm $NaYF_4$:Yb,Er/$NaYF_4$: 0.5% Er/PAAM with and without RB attached under 980 nm excitation. (e) Emission intensities of the UCNPs integrated in the range of 515−565 nm, and RB emission intensities integrated in the range of 565−630 nm from (a−d). (f) ET efficiency of UCNP/RB therapeutic agents calculated from (a−d) with the intensity of red emission as an internal reference.

in the shell are presented in Figure 4a. There were three emission peaks from Er^{3+} ions and a new emission peak centered at 590 nm, which originated from surface-anchored RB excited by the energy transferred from the UCNPs. The integrated emission intensities of RB anchored on the core/shell structured UCNPs relative to that on the core structured UCNPs are presented in Figure 4b. Compared with the core structured UCNPs, a proper shell coating improved the

https://doi.org/10.1021/acsanm.1c03377
ACS Appl. Nano Mater. 2022, 5, 559−568

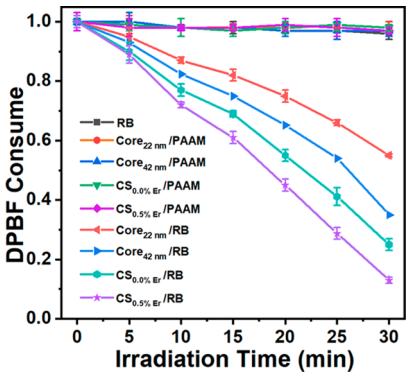

Figure 7. ROS production indicated by the decrease in DPBF absorbance at 417 nm under 980 nm irradiation.

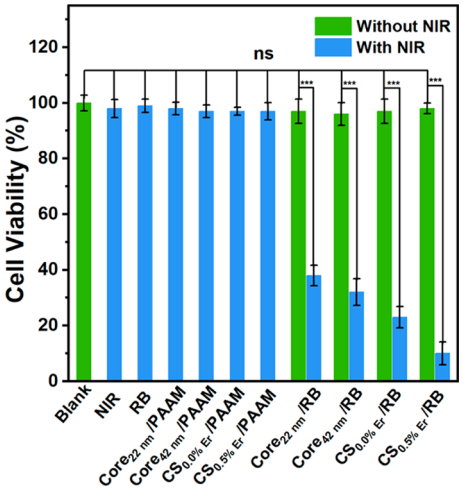

Figure 8. Viabilities of differently treated U87MG cells.

intensity of RB emission by one order of magnitude. The maximum RB emission intensity was achieved when 0.5% Er^{3+} ions were doped in the $NaYF_4$ shell. It was attributed to the ET-bridging effect of the Er^{3+} ions. ET efficiency (η) was calculated using $\eta = 1 - I_{DA}/I_D$, where I_{DA} and I_D are green emission intensities of UCNP/RB and UCNP/PAAM, respectively.[48] The ET efficiency from the core structured UCNPs to RB was the highest when the distance between the Er^{3+} emitters and RB was the shortest (Figure 4b). When a $NaYF_4$ shell with a thickness of ~5 nm was coated over the core, ET efficiency decreased markedly. It is because the Er^{3+} emitters in the core were far from the RB acceptors. When moderate amounts of Er^{3+} ions were introduced into the shell, the upconverted excitation energy from Er^{3+} ions in the core was able to migrate to the surface of the nanoparticles and further transfer to the RB photosensitizer. Thus, the ET efficiency increased distinctly. The slight decline in ET efficiency at high Er^{3+} concentrations can be ascribed to the reduced upconversion emission (Figure 2b) that shortens the ET interaction distance.[35,48] The results demonstrate that the core/emitter-active-shell structured UCNPs can enhance acceptor efficacy.

Thickness of the shell containing 0.5% Er^{3+} emitters was then adjusted to achieve the optimum RB efficacy. TEM images of the UCNPs with different shell thicknesses are presented in Figure S3. The average sizes of UCNPs from CS1 to CS8 were approximately 23, 27, 32, 34, 37, 42, 45, and 55 nm, respectively. The corresponding shell thickness was approximately 0.5, 2.5, 5, 6, 7.5, 10, 11.5, and 16.5 nm, respectively. As shell thickness increased, the upconversion luminescence intensity increased monotonically due to enhanced surface passivation (Figure S4). The upconversion luminescence spectra of the corresponding UCNP/RB therapeutic agents with various shell thicknesses are presented in Figure 5a, and the integrated RB emission intensities are shown in Figure 5b. The strongest RB emission occurred when the shell thickness was 10 nm (~42 nm in diameter). The RB emission was approximately 36 times that of the core counterpart. Therefore, the shell thickness can be optimized by balancing enhanced upconversion emission (Figure S4) and decreased ET efficiency (Figure S5). The remarkable enhancement of RB emission resulted from the synergistic effect of shell surface passivation and ET bridging by Er^{3+} ions.

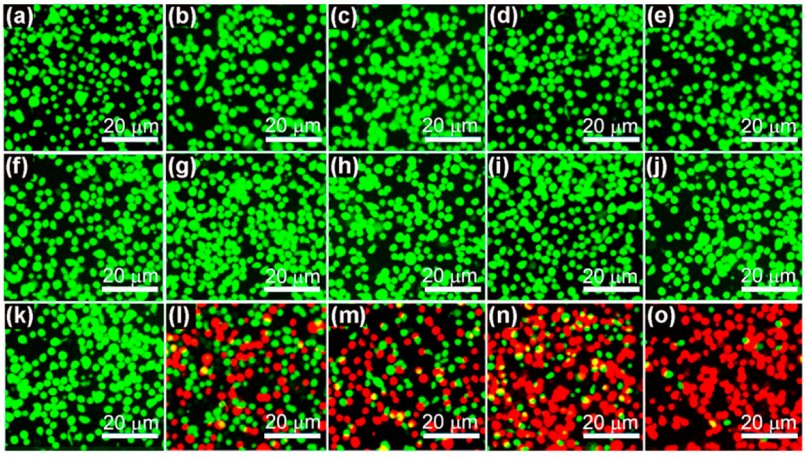

Figure 9. Fluorescence images of U87MG cells stained by calcein-AM (green, live cells) and PI (red, dead cells): (a) blank; (b) NIR irradiation; (c) RB, (d) ~22 nm $NaYF_4$:Yb,Er/PAAM, (e) ~42 nm $NaYF_4$:Yb,Er/PAAM, (f) ~42 nm $NaYF_4$:Yb,Er/$NaYF_4$/PAAM, and (g) ~42 nm $NaYF_4$:Yb,Er/$NaYF_4$:Er/PAAM under NIR irradiation; (h) ~22 nm $NaYF_4$:Yb,Er/RB, (i) ~42 nm $NaYF_4$:Yb,Er/RB, (j) ~42 nm $NaYF_4$:Yb,Er/$NaYF_4$/RB, and (k) ~42 nm $NaYF_4$:Yb,Er/$NaYF_4$:Er/RB without NIR irradiation; (l) ~22 nm $NaYF_4$:Yb,Er/RB, (m) ~42 nm $NaYF_4$:Yb,Er/RB, (n) ~42 nm $NaYF_4$:Yb,Er/$NaYF_4$/RB, and (o) ~42 nm $NaYF_4$:Yb,Er/$NaYF_4$:Er/RB under NIR irradiation. NIR irradiation has a power density of 0.70 W/cm^2 and an exposure time of 10 min.

https://doi.org/10.1021/acsanm.1c03377
ACS Appl. Nano Mater. 2022, 5, 559−568

3.2. Comparison of the RB Efficacy Excited by UCNPs with Different Structures. To further demonstrate the superiority of core/emitter-active-shell structure in improving acceptor efficacy, the intensity of the RB emission excited by the ∼42 nm $NaYF_4$:Yb,Er/$NaYF_4$:0.5% Er core/shell structured UCNPs was compared with that excited by other typically used UCNP structures (Figure 6a−d). In addition to the ∼22 nm $NaYF_4$:Yb,Er core used to construct core/emitter-active-shell structured UCNPs, $NaYF_4$:Yb,Er core and $NaYF_4$:Yb,Er/$NaYF_4$ core/inert-shell structured UCNPs with the same size (∼42 nm) as the core/emitter-active-shell structured UCNPs were also used. Although the upconversion luminescence of the ∼42 nm $NaYF_4$:Yb,Er core was approximately 14 times that of its ∼22 nm counterpart, it was still much lower than that of the $NaYF_4$:Yb,Er/$NaYF_4$: 0.5% Er core/shell structured UCNPs (Figure 6e). The enhanced upconversion luminescence and ET-bridging effect of Er^{3+} in the shell endowed $NaYF_4$:Yb,Er/$NaYF_4$: 0.5% Er with similar ET efficiency to the same-sized $NaYF_4$:Yb,Er core (Figure 6f). As a result, the RB emission intensity of $NaYF_4$:Yb,Er/$NaYF_4$: 0.5% Er/RB was much stronger than $NaYF_4$:Yb,Er/RB (Figure 6e). When a 10 nm $NaYF_4$ inert shell was coated on the ∼22 nm $NaYF_4$:Yb,Er UCNPs, the ET efficiency decreased markedly because the distance between the Er^{3+} emitters and the RB acceptors increased (Figure 6f). However, the RB emission intensity increased by approximately 13 times owing to the enhanced upconversion luminescence (Figure 6e). When 0.5% Er^{3+} was doped into the shell to bridge the ET between the Er^{3+} emitter and RB acceptor, the ET efficiency increased (Figure 6f). Simultaneously, the upconversion luminescence intensity further improved by 3.1 times (Figure 6e). Thus, the strongest RB emission was achieved with the $NaYF_4$:Yb,Er/$NaYF_4$: 0.5% Er core/shell structured UCNPs. It is worth noting that the ET efficiency calculated according to the quenched upconversion luminescence (Figure 6f) includes both radiative (reabsorption) and nonradiative (Förster resonance ET, i.e., FRET) pathways. The decay lifetimes of upconversion emission were further used to calculate the FRET efficiency by using $\eta_{FRET} = 1 - \tau_{DA}/\tau_D$, where τ_{DA} and τ_D are decay lifetimes of the green emission from UCNP/RB and UCNP/PAAM, respectively. Variation of FRET efficiency (Figure S6) was similar to that of total ET efficiency (Figure 6f). The significantly increased FRET efficiency of $NaYF_4$:Yb,Er/$NaYF_4$:Er/RB relative to $NaYF_4$:Yb,Er/$NaYF_4$/RB further demonstrates the ET-bridging effect of Er^{3+} doped in the shell.

The capability of the UCNP/RB therapeutic agents with various structures for producing ROS was then investigated using DPBF. The absorbance of DPBF at 417 nm decreases when it is oxidized by the produced ROS,[49] and therefore, this decrease in absorbance can be correlated to the amount of ROS produced. Figure 7 shows that the ROS was not generated when exposing RB or the UCNPs to the NIR light with a power density of 0.7 W/cm^2, which is below the safety threshold of a 980 nm laser.[50] When UCNP/RB therapeutic agents were irradiated using the 980 nm laser, ROS was produced. Variation trend of the amount of ROS was consistent with that of the RB emission intensity in Figure 6e. The $NaYF_4$:Yb,Er/$NaYF_4$: 0.5% Er core/shell UCNP/RB therapeutic agent produced the highest amount of ROS. Therefore, the core/emitter-active shell-structured UCNPs are more efficient than both core and core/inert-shell structured UCNPs in transferring energy to the RB acceptor.

3.3. Photodynamic Killing of Cancer Cells with UCNP/RB Therapeutic Agents. The intracellular ROS production and photodynamic performance of the UCNP/RB therapeutic agents were investigated using human glioblastoma cells (U87MG cell line). The stability of the UCNP/RB therapeutic agents was firstly evaluated. No noticeable precipitation occurred after UCNP/RB therapeutic agents were dispersed in water, PBS, and DMEM for one week (Figure S7). It indicated good stability of UCNP/RB therapeutic agents. Cytotoxicity of UCNP/RB therapeutic agents with four different UCNP structures was then evaluated using the CCK-8 method (Figure S8) and flow cytometry analysis (Figure S9). Both the methods showed cell viabilities of over 95% when the concentration of the UCNP/RB therapeutic agents reached 500 μg/mL, indicating their negligible cytotoxicity to U87MG cells at this concentration. Therefore, 500 μg/mL was used as the concentration of the UCNP/RB therapeutic agents in the following cell experiments. ROS production in the U87MG cells was observed with DCFH-DA, which reacted with ROS in the cells to produce green fluorescence under excitation.[51,52] Figure S10 shows fluorescence images of the cells under different treatments. The amount of ROS determined from the brightness of the green fluorescence agreed with that determined from the DPBF experiments (Figure 7). The core/emitter-active shell UCNP/RB therapeutic agent produced the most ROS for killing cancer cells.

The cell-killing effect of ROS produced by UCNP/RB therapeutic agents was then studied. It can be seen from Figure 8 that only the cells treated with both UCNP/RB therapeutic agents and NIR irradiation were killed efficiently, and more than 95% of the cells treated with RB or UCNPs and NIR irradiation remained alive. The cell mortality rate correlated with the amount of ROS produced by the UCNP/RB therapeutic agents with different structures. For the UCNP/RB therapeutic agents, the core/inert-shell UCNP structure killed cells more efficiently than the commonly used core UCNP structure, and the newly developed core/emitter-active shell UCNP structure further improved the cell mortality rate to 90%.

The photodynamic killing of glioma cells by the UCNP/RB therapeutic agents was further visualized using calcein-AM/PI staining (Figure 9. Green: live cells; red: dead cells). No dead cells appeared when the cells were treated with NIR irradiation only, NIR irradiation with RB or UCNPs, and UCNP/RB therapeutic agents only. However, dead cells were observed when the UCNP/RB therapeutic agents were used in combination with NIR exposure. The amount of dead cells correlated with the cell mortality rate under the same conditions (Figure 8). The UCNP/RB therapeutic agents with the core/emitter-active shell structure killed the most cancer cells under NIR irradiation.

4. CONCLUSIONS

In summary, an efficient NIR light-excitable photodynamic therapeutic agent was developed using $NaYF_4$:Yb,Er/$NaYF_4$:Er core/shell UCNPs and an RB photosensitizer. The core/shell UCNP/RB therapeutic agent with 0.5% Er^{3+} doped in a 10 nm shell exhibited the strongest RB emission, which was ∼36 times that of the core counterpart. This strong RB emission originated from surface passivation-induced upconversion luminescence enhancement and Er^{3+}-bridged efficient ET from the core of the UCNPs to the surface-bound RB

https://doi.org/10.1021/acsanm.1c03377
ACS Appl. Nano Mater. 2022, 5, 559−568

acceptor. Compared with the commonly used core and core/inert shell-structured UCNPs, the core/emitter-active shell structured UCNPs also endowed the RB photosensitizer with the most efficient ROS production capability under NIR irradiation. It was further demonstrated by photodynamic killing of glioma cells using UCNP/RB therapeutic agents. The results presented herein can facilitate the design of UCNP-based ET systems for broad applications in phototherapies, biosensing, optical storage, and so on.

■ ASSOCIATED CONTENT

Supporting Information

The Supporting Information is available free of charge at https://pubs.acs.org/doi/10.1021/acsanm.1c03377.

Reagents and instrumentation; DLS and inductively coupled plasma results of the UCNPs with various doping concentrations of Er in the shell; TEM images, emission spectra, and integrated emission intensities of the UCNPs with increasing shell thickness; ET efficiency of UCNP/RB therapeutic agents with different shell thicknesses; temporal behaviors of upconversion emission; digital photographs of the UCNP/RB therapeutic agents for various durations; cytotoxicity results of the UCNP/RB conjugates; and ROS detection results using DCFH-DA (PDF)

■ AUTHOR INFORMATION

Corresponding Authors

Yadan Ding − *Key Laboratory of UV-Emitting Materials and Technology (Northeast Normal University), Ministry of Education, Changchun 130024, China;* orcid.org/0000-0001-6608-2297; Email: dingyd044@nenu.edu.cn

Xia Hong − *Key Laboratory of UV-Emitting Materials and Technology (Northeast Normal University), Ministry of Education, Changchun 130024, China;* orcid.org/0000-0002-8166-6562; Email: xiahong@nenu.edu.cn

Hong Zhang − *Van't Hoff Institute for Molecular Sciences, University of Amsterdam, Amsterdam 1098 XH, The Netherlands*; Email: h.zhang@uva.nl

Authors

Jie Ren − *Key Laboratory of UV-Emitting Materials and Technology (Northeast Normal University), Ministry of Education, Changchun 130024, China*

Hancheng Zhu − *Key Laboratory of UV-Emitting Materials and Technology (Northeast Normal University), Ministry of Education, Changchun 130024, China*

Zhipeng Li − *Key Laboratory of UV-Emitting Materials and Technology (Northeast Normal University), Ministry of Education, Changchun 130024, China*

Rui Dai − *Key Laboratory of UV-Emitting Materials and Technology (Northeast Normal University), Ministry of Education, Changchun 130024, China*

Huiying Zhao − *Department of Basic Medicine, Gerontology Department of First Bethune Hospital, University of Jilin, Changchun, Jilin 130021, China*

Complete contact information is available at: https://pubs.acs.org/10.1021/acsanm.1c03377

Notes

The authors declare no competing financial interest.

■ ACKNOWLEDGMENTS

This work was supported by the National Natural Science Foundation of China (51972052, 11604043, 11604044, 51772122, and 11674316), the Scientific and Technological Developing Scheme of Jilin province (20190201243JC), the Science and Technology Research Project of Education Department of Jilin province (JJKH20211275KJ), the Fundamental Research Funds for the Central Universities (2412019FZ033), the 111 Project (B13013), the Netherlands Organization for Scientific Research in the framework of the Fund New Chemical Innovation (731.015.206), and the EU H2020-MSCA-RISE Action program, CANCER (777682).

■ REFERENCES

(1) Lan, M.; Zhao, S.; Liu, W.; Lee, C. S.; Zhang, W.; Wang, P. Photosensitizers for Photodynamic Therapy. *Adv. Healthcare Mater.* **2019**, *8*, 1900132.

(2) Chen, D.; Xu, Q.; Wang, W.; Shao, J.; Huang, W.; Dong, X. Type I Photosensitizers Revitalizing Photodynamic Oncotherapy. *Small* **2021**, *17*, 2006742.

(3) Wei, F.; Rees, T. W.; Liao, X.; Ji, L.; Chao, H. Oxygen Self-Sufficient Photodynamic Therapy. *Coord. Chem. Rev.* **2021**, *432*, 213714.

(4) Keerthiga, R.; Zhao, Z.; Pei, D.; Fu, A. Photodynamic Nanophotosensitizers: Promising Materials for Tumor Theranostics. *ACS Biomater. Sci. Eng.* **2020**, *6*, 5474−5485.

(5) Agostinis, P.; Berg, K.; Cengel, K. A.; Foster, T. H.; Girotti, A. W.; Gollnick, S. O.; Hahn, S. M.; Hamblin, M. R.; Juzeniene, A.; Kessel, D.; Korbelik, M.; Moan, J.; Mroz, P.; Nowis, D.; Piette, J.; Wilson, B. C.; Golab, J. Photodynamic Therapy of Cancer: An Update. *Ca-Cancer J. Clin.* **2011**, *61*, 250−281.

(6) Wang, X.; Li, Z.; Ding, Y.; Wang, K.; Xing, Z.; Sun, X.; Guo, W.; Hong, X.; Zhu, X.; Liu, Y. Enhanced Photothermal-Photodynamic Therapy for Glioma Based on Near-Infrared Dye Functionalized Fe_3O_4 Superparticles. *Chem. Eng. J.* **2020**, *381*, 122693.

(7) Wan, Y.; Lu, G.; Wei, W.-C.; Huang, Y.-H.; Li, S.; Chen, J.-X.; Cui, X.; Xiao, X.; Liu, Y.; Meng, X.-M.; Wang, P.; Xie, H.-Y.; Zhang, J.; Wong, K.-T.; Lee, C.-S. Stable Organic Photosensitizer Nanoparticles with Absorption Peak Beyond 800 Nanometers and High Reactive Oxygen Species Yield for Multimodality Phototheranostics. *ACS Nano* **2020**, *14*, 9917−9928.

(8) Lucky, S. S.; Soo, K. C.; Zhang, Y. Nanoparticles in Photodynamic Therapy. *Chem. Rev.* **2015**, *115*, 1990−2042.

(9) Feng, Y.; Chen, H.; Wu, Y.; Que, I.; Tamburini, F.; Baldazzi, F.; Chang, Y.; Zhang, H. Optical Imaging and pH-Awakening Therapy of Deep Tissue Cancer Based on Specific Upconversion Nanophotosensitizers. *Biomaterials* **2020**, *230*, 119637.

(10) Lahtinen, S.; Liisberg, M. B.; Raiko, K.; Krause, S.; Soukka, T.; Vosch, T. Thulium- and Erbium-Doped Nanoparticles with Poly(acrylic acid) Coating for Upconversion Cross-Correlation Spectroscopy-based Sandwich Immunoassays in Plasma. *ACS Appl. Nano Mater.* **2021**, *4*, 432−440.

(11) Li, X.; Zhang, F.; Zhao, D. Lab on Upconversion Nanoparticles: Optical Properties and Applications Engineering via Designed Nanostructure. *Chem. Soc. Rev.* **2015**, *44*, 1346−1378.

(12) Soni, A. K.; Joshi, R.; Singh, B. P.; Kumar, N. N.; Ningthoujam, R. S. Near-Infrared- and Magnetic-Field-Responsive $NaYF_4:Er^{3+}/Yb^{3+}@SiO_2@AuNP@Fe_3O_4$ Nanocomposites for Hyperthermia Applications Induced by Fluorescence Resonance Energy Transfer and Surface Plasmon Absorption. *ACS Appl. Nano Mater.* **2019**, *2*, 7350−7361.

(13) Wang, S.; Bi, A.; Zeng, W.; Cheng, Z. Upconversion Nanocomposites for Photo-Based Cancer Theranostics. *J. Mater. Chem. B* **2016**, *4*, 5331−5348.

(14) Liu, Y.; Meng, X.; Bu, W. Upconversion-Based Photodynamic Cancer Therapy. *Coord. Chem. Rev.* **2019**, *379*, 82−98.

(15) Loo, J. F.-C.; Chien, Y.-H.; Yin, F.; Kong, S.-K.; Ho, H.-P.; Yong, K.-T. Upconversion and Downconversion Nanoparticles for Biophotonics and Nanomedicine. *Coord. Chem. Rev.* **2019**, *400*, 213042.
(16) Wang, X.; Yang, C.-X.; Chen, J.-T.; Yan, X.-P. A Dual-Targeting Upconversion Nanoplatform for Two-Color Fluorescence Imaging-Guided Photodynamic Therapy. *Anal. Chem.* **2014**, *86*, 3263−3267.
(17) Idris, N. M.; Gnanasammandhan, M. K.; Zhang, J.; Ho, P. C.; Mahendran, R.; Zhang, Y. In Vivo Photodynamic Therapy using Upconversion Nanoparticles as Remote-Controlled Nanotransducers. *Nat. Med.* **2012**, *18*, 1580−1585.
(18) Zhang, Q.; Wang, W.; Zhang, M.; Wu, F.; Zheng, T.; Sheng, B.; Liu, Y.; Shen, J.; Zhou, N.; Sun, Y. A Theranostic Nanocomposite with Integrated Black Phosphorus Nanosheet, Fe_3O_4@MnO_2-Doped Upconversion Nanoparticles and Chlorin for Simultaneous Multimodal Imaging, Highly Efficient Photodynamic and Photothermal Therapy. *Chem. Eng. J.* **2020**, *391*, 123525.
(19) Chen, X.; Peng, D.; Ju, Q.; Wang, F. Photon Upconversion in Core-Shell Nanoparticles. *Chem. Soc. Rev.* **2015**, *44*, 1318−1330.
(20) Vetrone, F.; Naccache, R.; Mahalingam, V.; Morgan, C. G.; Capobianco, J. A. The Active-Core/Active-Shell Approach: a Strategy to Enhance the Upconversion Luminescence in Lanthanide-Doped Nanoparticles. *Adv. Funct. Mater.* **2009**, *19*, 2924−2929.
(21) Boyer, J.-C.; Van Veggel, F. C. J. M. Absolute Quantum Yield Measurements of Colloidal $NaYF_4$: Er^{3+}, Yb^{3+} Upconverting Nanoparticles. *Nanoscale* **2010**, *2*, 1417−1419.
(22) Lv, R.; Feng, M.; Liu, J.; Jiang, X.; Yuan, H.; Yan, R.; Tian, J. Improved Red Emission and Short-Wavelength Infrared Luminescence under 808 nm Laser for Tumor Theranostics. *ACS Biomater. Sci. Eng.* **2019**, *5*, 4683−4691.
(23) Ding, Y.; Wu, F.; Zhang, Y.; Liu, X.; de Jong, E. M. L. D.; Gregorkiewicz, T.; Hong, X.; Liu, Y.; Aalders, M. C. G.; Buma, W. J.; Zhang, H. Interplay Between Static and Dynamic Energy Transfer in Biofunctional Upconversion Nanoplatforms. *J. Phys. Chem. Lett.* **2015**, *6*, 2518−2523.
(24) Wang, Y.; Liu, K.; Liu, X.; Dohnalová, K.; Gregorkiewicz, T.; Kong, X.; Aalders, M. C. G.; Buma, W. J.; Zhang, H. Critical Shell Thickness of Core/Shell Upconversion Luminescence Nanoplatform for FRET Application. *J. Phys. Chem. Lett.* **2011**, *2*, 2083−2088.
(25) Tajon, C. A.; Yang, H.; Tian, B.; Tian, Y.; Ercius, P.; Schuck, P. J.; Chan, E. M.; Cohen, B. E. Photostable and Efficient Upconverting Nanocrystal-Based Chemical Sensors. *Opt. Mater.* **2018**, *84*, 345−353.
(26) Labrador-Páez, L.; Ximendes, E. C.; Rodríguez-Sevilla, P.; Ortgies, D. H.; Rocha, U.; Jacinto, C.; Martín Rodríguez, E.; Haro-González, P.; Jaque, D. Core-Shell Rare-Earth-Doped Nanostructures in Biomedicine. *Nanoscale* **2018**, *10*, 12935−12956.
(27) Pham, K.-Y.; Wang, L.-C.; Hsieh, C.-C.; Hsu, Y.-P.; Chang, L.-C.; Su, W.-P.; Chien, Y.-H.; Yeh, C.-S. 1550 nm Excitation-Responsive Upconversion Nanoparticles to Establish Dual-Photodynamic Therapy Against Pancreatic Tumors. *J. Mater. Chem. B* **2021**, *9*, 694−709.
(28) Hou, Z.; Deng, K.; Li, C.; Deng, X.; Lian, H.; Cheng, Z.; Jin, D.; Lin, J. 808 nm Light-Triggered and Hyaluronic Acid-Targeted Dual-Photosensitizers Nanoplatform by Fully Utilizing Nd^{3+}-Sensitized Upconversion Emission with Enhanced Anti-Tumor Efficacy. *Biomaterials* **2016**, *101*, 32−46.
(29) Zhang, X.; Ai, F.; Sun, T.; Wang, F.; Zhu, G. Multimodal Upconversion Nanoplatform with a Mitochondria-Targeted Property for Improved Photodynamic Therapy of Cancer Cells. *Inorg. Chem.* **2016**, *55*, 3872−3880.
(30) Yang, M.; Wang, H.; Wang, Z.; Han, Z.; Gu, Y. A Nd^{3+} Sensitized Upconversion Nanosystem with Dual Photosensitizers for Improving Photodynamic Therapy Efficacy. *Biomater. Sci.* **2019**, *7*, 1686−1695.
(31) Xu, J.; Lv, R.; Du, S.; Gai, S.; He, F.; Yang, D.; Yang, P. UCNPs@Gelatin-ZnPc Nanocomposite: Synthesis, Imaging and Anticancer Properties. *J. Mater. Chem. B* **2016**, *4*, 4138−4146.
(32) Sun, Q.; He, F.; Sun, C.; Wang, X.; Li, C.; Xu, J.; Yang, D.; Bi, H.; Gai, S.; Yang, P. Honeycomb-Satellite Structured pH/H_2O_2-Responsive Degradable Nanoplatform for Efficient Photodynamic Therapy and Multimodal Imaging. *ACS Appl. Mater. Interfaces* **2018**, *10*, 33901−33912.
(33) Shao, Y.; Liu, B.; Di, Z.; Zhang, G.; Sun, L.-D.; Li, L.; Yan, C.-H. Engineering of Upconverted Metal-Organic Frameworks for Near-Infrared Light-Triggered Combinational Photodynamic/Chemo-/Immunotherapy Against Hypoxic tumors. *J. Am. Chem. Soc.* **2020**, *142*, 3939−3946.
(34) Kumar, N.; Su, W. T.; Vesel, M.; Weckhuysen, B. M.; Pollard, A. J.; Wain, A. J. Nanoscale Chemical Imaging of Solid-Liquid Interfaces Using Tip-Enhanced Raman Spectroscopy. *Nanoscale* **2018**, *10*, 1815.
(35) Marin, R.; Labrador-Paéz, L.; Skripka, A.; Haro-González, P.; Benayas, A.; Canton, P.; Jaque, D.; Vetrone, F. Upconverting Nanoparticle to Quantum Dot Förster Resonance Energy Transfer: Increasing the Efficiency through Donor Design. *ACS Photonics* **2018**, *5*, 2261−2270.
(36) Bhuckory, S.; Hemmer, E.; Wu, Y. T.; Yahia-Ammar, A.; Vetrone, F.; Hildebrandt, N. Core or Shell? Er^{3+} FRET Donors in Upconversion Nanoparticles. *Eur. J. Inorg. Chem.* **2017**, *2017*, 5186−5195.
(37) Lin, S.-L.; Chen, H.-C.; Chang, C. A. Enhancing Förster Resonance Energy Transfer (FRET) Efficiency of Titania-Lanthanide Hybrid Upconversion Nanomaterials by Shortening the Donor-Acceptor Distance. *Nanomaterials* **2020**, *10*, 2035.
(38) Siefe, C.; Mehlenbacher, R. D.; Peng, C. S.; Zhang, Y.; Fischer, S.; Lay, A.; McLellan, C. A.; Alivisatos, A. P.; Chu, S.; Dionne, J. A. Sub-20 nm Core-Shell-Shell Nanoparticles for Bright Upconversion and Enhanced Förster Resonant Energy Transfer. *J. Am. Chem. Soc.* **2019**, *141*, 16997−17005.
(39) Lin, S.-L.; Chang, C. A. Optimising FRET-Efficiency of Nd^{3+}-Sensitised Upconversion Nanocomposites by Shortening the Emitter-Photosensitizer Distance. *Nanoscale* **2020**, *12*, 8742−8749.
(40) Johnson, N. J. J.; Korinek, A.; Dong, C.; van Veggel, F. C. J. M. Self-Focusing by Ostwald Ripening: a Strategy for Layer-by-Layer Epitaxial Growth on Upconverting Nanocrystals. *J. Am. Chem. Soc.* **2012**, *134*, 11068−11071.
(41) Neckers, D. C.; Paczkowski, J. Micro-organizational control of photochemical oxidations: Rose bengal and derivatives (XV). *Tetrahedron* **1986**, *42*, 4671−4683.
(42) Qian, H.-S.; Zhang, Y. Synthesis of Hexagonal-Phase Core-Shell $NaYF_4$ Nanocrystals with Tunable Upconversion Fluorescence. *Langmuir* **2008**, *24*, 12123−12125.
(43) Li, Z.; Zhang, Y. An Efficient and User-Friendly Method for the Synthesis of Hexagonal-Phase $NaYF_4$:Yb, Er/Tm Nanocrystals with Controllable Shape and Upconversion Fluorescence. *Nanotechnol* **2008**, *19*, 345606.
(44) Wang, F.; Han, Y.; Lim, C. S.; Lu, Y.; Wang, J.; Xu, J.; Chen, H.; Zhang, C.; Hong, M.; Liu, X. Simultaneous Phase and Size Control of Upconversion Nanocrystals through Lanthanide Doping. *Nature* **2010**, *463*, 1061−1065.
(45) Li, H.; Shi, X.; Li, X.; Zong, L. Size-Tunable β-$NaYF_4$:Yb/Er Up-Converting Nanoparticles with a Strong Green Emission Synthesized by Thermal Decomposition. *Opt. Mater.* **2020**, *108*, 110144.
(46) Homann, C.; Krukewitt, L.; Frenzel, F.; Grauel, B.; Würth, C.; Resch-Genger, U.; Haase, M. $NaYF_4$:Yb,Er/$NaYF_4$ Core/Shell Nanocrystals with High Upconversion Luminescence Quantum Yield. *Angew. Chem., Int. Ed.* **2018**, *57*, 8765−8769.
(47) Wang, F.; Wang, J.; Liu, X. Direct Evidence of a Surface Quenching Effect on Size-Dependent Luminescence of Upconversion Nanoparticles. *Angew. Chem., Int. Ed.* **2010**, *49*, 7456−7460.
(48) Dukhno, O.; Przybilla, F.; Collot, M.; Klymchenko, A.; Pivovarenko, V.; Buchner, M.; Muhr, V.; Hirsch, T.; Mély, Y. Quantitative Assessment of Energy Transfer in Upconverting Nanoparticles Grafted with Organic Dyes. *Nanoscale* **2017**, *9*, 11994−12004.
(49) Lu, S.; Tu, D.; Hu, P.; Xu, J.; Li, R.; Wang, M.; Chen, Z.; Huang, M.; Chen, X. Multifunctional Nano-Bioprobes Based on

https://doi.org/10.1021/acsanm.1c03377
ACS Appl. Nano Mater. 2022, 5, 559−568

Rattle-Structured Upconverting Luminescent Nanoparticles. *Angew. Chem., Int. Ed.* **2015**, *54*, 7915−7919.
(50) Chen, G.; Ågren, H.; Ohulchanskyy, T. Y.; Prasad, P. N. Light Upconverting Core-Shell Nanostructures: Nanophotonic Control for Emerging Applications. *Chem. Soc. Rev.* **2015**, *44*, 1680−1713.
(51) Li, Z.; Qiao, X.; He, G.; Sun, X.; Feng, D.; Hu, L.; Xu, H.; Xu, H.-B.; Ma, S.; Tian, J. Core-Satellite Metal-Organic Framework@ Upconversion Nanoparticle Superstructures via Electrostatic Self-Assembly for Efficient Photodynamic Theranostics. *Nano Res.* **2020**, *13*, 3377−3386.
(52) Jin, F.; Qi, J.; Zhu, M.; Liu, D.; You, Y.; Shu, G.; Du, Y.; Wang, J.; Yu, H.; Sun, M.; Xu, X.; Shen, Q.; Ying, X.; Ji, J.; Du, Y. NIR-Triggered Sequentially Responsive Nanocarriers Amplified Cascade Synergistic Effect of Chemo-Photodynamic Therapy with Inspired Antitumor Immunity. *ACS Appl. Mater. Interfaces* **2020**, *12*, 32372−32387.

https://doi.org/10.1021/acsanm.1c03377
ACS Appl. Nano Mater. 2022, 5, 559−568